Aerosol and Air Quality Research, 19: 2196–2204, 2019

ISSN: 1680-8584 print / 2071-1409 online
doi: 10.4209/aaqr.2019.08.0388

Effects of Operating Parameters on Gas-phase PAH Emissions from a Direct Methanol Fuel Cell

Kuo-Lin Huang*, Yu-Hsien Liao, Shui-Jen Chen

Department of Environmental Engineering and Science, National Pingtung University of Science and Technology, Pingtung 91201, Taiwan

ABSTRACT

This study aims at investigating the emissions of cathode gas-phase polycyclic aromatic hydrocarbons (PAHs) from a single direct methanol fuel cell (DMFC) at different operating parameters (methanol concentration, methanol flowrate, oxygen flowrate, and cell temperature). At the standard test condition (run A1), the concentrations of stage 1 (S1) and S2 PAHs ranged from non-detect (ND) to 10.3 ± 2.54 (Nap) and ND to 0.148 ± 0.047 (IND) μg Nm^{-3}, respectively; furthermore, the Total-PAHs and Total-BaP_{eq} concentrations of S1 + S2 were 21.2 ± 4.48 μg Nm^{-3} and 409 ± 226 ng Nm^{-3}, respectively. The operating parameters significantly influenced the patterns of PAH concentration profiles. Decreasing with increasing methanol flowrate and concentration or decreasing oxygen flowrate and cell temperature, the ranges of Total-PAHs and Total-BaP_{eq} concentrations of S1 + S2 for different runs were (36.4 ± 10.9)–(0.98 ± 0.21) μg Nm^{-3} and (409 ± 226)–(98.7 ± 30.3) ng Nm^{-3}, respectively, with corresponding emission factors from 0.07 ± 0.03 to 2.44 ± 0.52 μg g-$electrode^{-1}$ and from 7.58 ± 2.32 to 47.1 ± 26.0 ng g-$electrode^{-1}$, respectively. At the same operating condition, more cathode gas-phase Total-PAHs and Total-BaP_{eq} emissions were observed for the DMFC using a HE membrane-electrode assembly (MEA) than for using an E-TEK MEA. The DMFC had the lowest performance when the cell temperature was 60°C.

Keywords: Polycyclic aromatic hydrocarbon (PAH); Direct methanol fuel cell; Emission factor; Gas-phase PAH.

INTRODUCTION

The use of polymer electrolyte membrane fuel cells (PEMFCs) in the transport and other sectors for power generation may alleviate the consumption of fossil fuels along with its atmospheric emission of greenhouse gases (mainly carbon dioxide) and air pollutants, such as nitrogen oxides, sulfur oxides, volatile organic compounds, particulate matter, and others (Kumar *et al.*, 2014; Joghee *et al.*, 2015). As one kind of PEMFCs, direct methanol fuel cells (DMFCs), enabling the direct conversion of the chemical energy stored in liquid methanol fuel to electrical energy with main by-products of water and carbon dioxide, are advantageous in power supply of transportation (without on-board storage constraints) (Joghee *et al.*, 2015) and portable electronic devices (Joghee *et al.*, 2015; Deng *et al.*, 2019). However, in comparison to H_2-based fuel cells, DMFCs suffer from challenges such as lower efficiency, lower power density, and higher cost, which impede their commercialization, although the DMFC technology has great potential for commercialization to power small portable appliances (Joghee *et al.*, 2015).

A DMFC normally has a membrane-electrode assembly (MEA) symmetrically sandwiched by two Telfon gaskets, two carbon (graphite) blocks (with gas flow channels), two copper current collectors, and two aluminum end plates (Bahrami and Faghri, 2013; Tiwari *et al.*, 2013; Falcão *et al.*, 2014). It is common for an acid-based DMFC to use an MEA which consists of a polymer electrolyte (or proton exchange) membrane (PEM), anode catalyst layer on gas diffusion layer (GDL), and cathode catalyst layer on cathode GDL (Bahrami and Faghri, 2013). Accordingly, the structure of an acid type DMFC can be depicted as Fig. 1. Moreover, the main electrochemical reactions at anode and cathode are methanol oxidation (reaction 1) (E^0 = 0.016 V vs. standard hydrogen electrode (SHE)) and oxygen reduction (reaction 2) (E^0 = 1.229 V vs. SHE), respectively (Tiwari *et al.*, 2013).

$$CH_3OH + H_2O \rightarrow CO_2 + 6H^+ + 6e^- \quad (1)$$

$$1.5O_2 + 6H^+ + 6e^- \rightarrow 3H_2O \quad (2)$$

Therefore, the overall reaction (E^0 = 1.21 V vs. SHE) can be shown as follows:

$$CH_3OH + 1.5O_2 \rightarrow CO_2 + 2H_2O \quad (3)$$

* Corresponding author.
Tel.: +886-8-7703202 ext. 7092; Fax: +886-8-7740256
E-mail address: huangkL@mail.npust.edu.tw

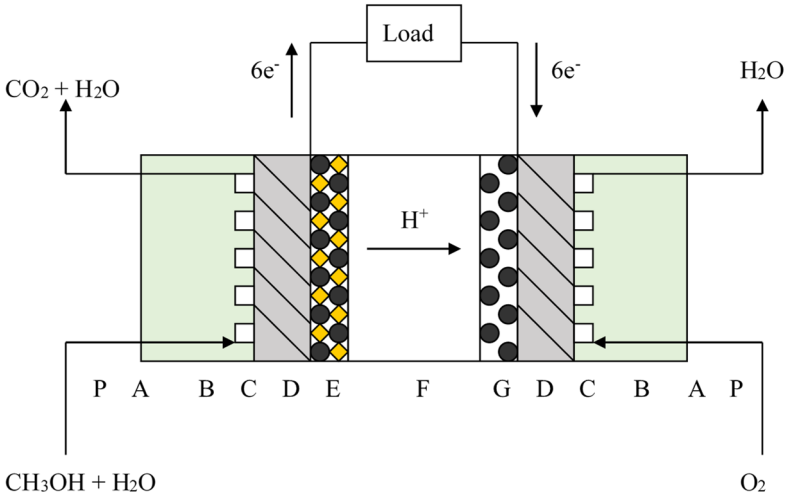

Fig. 1. The scheme of single DMFC with symmetrical components (A: current collector, B: graphite block, C: flow channel, D: gas diffusion layer, E: PtRu anode, F: Nafion membrane, G: Pt cathode, and P: end plate) (MEA: D + E + F + G + D).

To enhance methanol oxidation activity and minimize CO poisoning, PtRu is more frequently used than other Pt-based binary alloys as the anode catalyst for DMFCs (Tiwari *et al.*, 2013; Mansor *et al.*, 2019), while Pt is more often to be adopted as the cathode catalyst than Pd and Au or binary metals (Tiwari *et al.*, 2013). Various carbon materials such as functionalized mesoporous carbon, activated carbon nanotube, graphene, carbon nanofiber, and carbon nanosphere) are candidates for being used to support anode and cathode catalysts (Tiwari *et al.*, 2013; Tsukagoshi *et al.*, 2018; Mansor *et al.*, 2019), while carbon blacks are often used for the fabrication of bipolar/end plates and GDLs (e.g., carbon paper or cloth) (Tran *et al.*, 2015; Zeis, 2015; Lee and Lee, 2016).

According to reaction 1, CO_2 will be generated from the methanol oxidation at anode during the operation of DMFC (Li and Faghri, 2013; Tiwari *et al.*, 2013), although they are considered as environmental friendly due to less air pollutant emissions, in comparison to gasoline-powered vehicles (Joghee *et al.*, 2015). Additionally, DMFCs probably might emit some toxic byproducts, such as formic acid, methylformate, formaldehyde, and methylal) (Wasmus and Küver, 1999; Nakagawa *et al.*, 2009). Therefore, more fundamental research is necessary to make DMFC technology more appealing and the DMFC systems more competitive in the portable power market (Li and Faghri, 2013).

Our earlier works reported the emissions of polycyclic aromatic hydrocarbons (PAHs) originally absorbed on carbon materials from a H_2-O_2 PEMFC which is usually claimed for power generation with zero emission (Huang *et al.*, 2015; Huang *et al.*, 2016; Huang *et al.*, 2018). Polycyclic aromatic hydrocarbons (PAHs) having chemical structures with two or more benzene rings are generated from natural combustion or anthropogenic activities such as incomplete combustion and/or pyrosynthesis of organic compounds (Li *et al.*, 2017; Siudek and Frankowski, 2018). Long been concerned for adverse impacts on health and the environment, PAHs can be generated from various sources (e.g., domestic combustion, vehicle exhaust, industry and power stations) (Mario *et al.*, 2018), and are now widely distributed in the global atmosphere, particularly in that of populated and industrial regions (Fan *et al.*, 2017; Lai *et al.*, 2017; Li *et al.*, 2017; Saha *et al.*, 2017; Wang *et al.*, 2017; Dat *et al.*, 2018; Jiang *et al.*, 2018; Wright *et al.*, 2018; Xu *et al.*, 2018; Zhang *et al.*, 2018). To minimize the adverse effects of methanol crossover, it is common that the methanol concentrations used for active and passive DMFCs are 1–2 M (3–6 wt%) and ~3 M (10 wt%), respectively, at tested temperature = 60–120°C and suitable stoichiometric methanol to O_2 flowrate ratios (Li and Faghri, 2013; Joghee *et al.*, 2015). In addition to methanol concentration and cell temperature, other operating parameters such as anode methanol and cathode oxygen flowrates may influence the emission of byproducts or pollutants from a DMFC. However, little attention has been paid to the emission of PAHs from DMFCs. In this study, we explored the emissions gas-phase PAHs and BaPeq from a DMFC under different anode methanol and cathode oxygen flowrates, methanol concentrations, and temperatures.

MATERIALS AND METHODS

Membrane-Electrode Assembly (MEA) and Fuel Cell Emission Test

The tested membrane-electrode assemblies (MEAs) were mostly purchased from Hephas Energy (HE) Co., Ltd. Each HE MEA, consisted of a proton exchange membrane (PEM) (solid electrolyte) (Nafion-115) sandwiched with two dispersed catalyst layers and gas diffusion layers (GDLs), had an anode PtRu loading of 3 mg cm^{-2} and a cathode Pt loading of 0.3 mg cm^{-2}. For comparison, E-TEK MEAs were also tested. The PEM, anode catalyst loading, and cathode catalyst loading of each E-TEK MEA were Nafion–117, 4 mg-PtRu cm^{-2} and 4 mg-Pt cm^{-2}, respectively. The structure of MEA was reported in our earlier papers (Huang *et al.*, 2006; Lai *et al.*, 2012; Huang *et al.*, 2015, 2016, 2018).

In this study, the tested DMFC had components of MEA, carbon blocks, and copper current collectors serially

connected together as shown in Fig. 1. Installed on a standard fuel cell test station, the DMFC was run at 0.3 V (cathode humidification temperature = 40°C) for 6.4 h and then another 6.4 h for stages 1 and 2 (S1 and S2) PAH samplings, respectively, under different anode methanol flow rates (2 and 10 mL min^{-1}), methanol concentration (2 and 4 M), cathode oxygen flow rates (100 and 150 sccm) and temperatures (60°C and 80°C). The tested operating parameters of different runs (A1, B, C, D, E, and A2) are summarized in Table 1. For comparing PAHs emission using different MEAs, the runs A1 (HE MEA) and A2 (E-TEK MEA) had the same operating conditions: methanol concentration = 2 M, methanol flowrate = 2 mL min^{-1}, oxygen flowrate = 150 sccm, and cell temperature = 80°C. Moreover, the run A1 is denoted as the standard test condition. A potentiostat (CHI 660A Electrochemical Analyzer) plus PC system connected with the test station was used to perform the AC impedance measurements for methanol oxidation and oxygen reduction reactions in the frequency range of 10 K to 0.01 Hz (10 mV amplitude) at 0.5 V using the oxygen-feeding cathode (working electrode) and methanol-feeding anode (counter electrode).

PAH Sampling, Analysis, and Quality Control

During cell operation, a peristaltic pump (ChromTech TP-320) was used to circulate the anode fuel (methanol) between the anode and a reservoir, while the cathode-feeding gas was oxygen and its flowrate was regulated by a mass flow controller. The gas-phase PAH samples were collected from the cathode emission port connected with a glass cartridge which was packed with XAD-16 resin granules and supported by a polyurethane foam (PUF) plug. Similar cathode sampling systems for PAH collection were also addressed in our previous works (Huang *et al.*, 2015, 2016, 2018).

For each experiment, triplicate PAH samplings (n = 3) were performed. After PAH collection, cell polarization tests were performed at different anode/cathode flowrates or cell temperatures. The tested 21 PAH species were: naphthalene (Nap), acenaphthylene (AcPy), acenaphthene (Acp), fluorene (Flu), phenanthrene (PA), anthracene (Ant), fluoranthene (FL), pyrene (Pyr), benzo(a)anthracene (BaA), chrysene (CHR), cyclopenta(c,d)pyrene (CYC), benzo(b)fluoranthene (BbF), benzo(k)fluoranthene (BkF), benzo(e)pyrene (BeP), benzo(a)pyrene (BaP), perylene (PER), indeno(1,2,3,-cd)pyrene (IND), dibenzo(a,h)anthrance (DBA), benzo(b)chrycene (BbC), benzo(ghi)perylene (BghiP), and coronene (COR). These PAH species were classified into three categories: low molecular weight (LMW-PAHs, 2-/3-ring PAHs: NaP, AcPy, AcP, Flu, Ant, and PA), middle molecular weight (MMW-PAHs, 4-ring PAHs: FL, Pyr, BaA, and CHR), and high molecular weight (HMW-PAHs, 5-/6-/7-ring PAHs: CYC, BbF, BkF, BeP, BaP, PER, DBA, BbC, IND, BghiP, and COR). The Total-PAHs concentration was obtained from the sum of the concentrations of 21 PAH species.

One of our earlier papers provided the details of PAHs extraction by Soxhlet extraction method, the identification/quantification of PAHs (with blank correction) by gas chromatograph/mass spectrometry (GC/MS), and the quality assurance (QA)/quality control (QC) procedures for PAHs GC/MS analysis (Huang *et al.*, 2015). The correlation coefficients of the calibration curves were 0.994–0.999. The average relative standard deviation (RSD) of the GC/MS integration area was 3.0% with a range of 0.8–5.1% in ten consecutive injections of a PAH 610-M standard. Through seven consecutive injections, the range of total recovery efficiencies of PAHs was from 83% to 112%, while the average recoveries of the five internal standards were 85–93%.

The coefficients of variation for repeat injections of the standard solution (containing PAH Mixture-610 M (16 PAHs)

Table 1. Operating conditions (OPs: methanol concentration, methanol flowrate, O_2 flowrate, and cell temperature); gas-phase Total-PAHs concentrations and Total-BaP_{eq} concentrations and emission factors (EFs) for the stage 1 (S1), stage 2 (S2), and sums (S1 + S2) at different runs.

Run	Methanol conc. (M)	Methanol flowrate (mL min^{-1})	O_2 flowrate (sccm)	Cell temp. (°C)	Total-PAHs S1 + S2 (μg Nm^{-3})	Total-BaP_{eq} S1 + S2 (ng Nm^{-3})
A1	2	2	150	80	21.2 ± 4.48	409 ± 226
B	2	10	150	80	3.31 ± 0.43	102 ± 32.6
C	4	2	150	80	9.68 ± 3.44	102 ± 40.7
D	2	2	100	80	0.98 ± 0.21	98.7 ± 30.3
E	2	2	150	60	7.98 ± 3.85	257 ± 51.7
A2	2	2	150	80	36.4 ± 10.9	82.3 ± 35.3

EFs	Total-PAHs (μg g-electrode^{-1})			Total-BaP_{eq} (ng g-electrode^{-1})		
	S1	S2	S1 + S2	S1	S2	S1 + S2
A1	2.38 ± 0.52	0.06 ± 0.02	2.44 ± 0.52	30.8 ± 22.8	16.3 ± 12.5	47.1 ± 26.0
B	0.07 ± 0.04	0.31 ± 0.02	0.38 ± 0.05	2.42 ± 1.96	9.34 ± 3.20	11.8 ± 3.75
C	0.81 ± 1.00	0.31 ± 0.24	1.12 ± 1.03	6.93 ± 2.94	4.78 ± 3.65	11.7 ± 4.68
D	0.06 ± 0.02	0.01 ± 0.02	0.07 ± 0.03	7.03 ± 2.21	0.55 ± 0.71	7.58 ± 2.32
E	0.23 ± 0.09	0.69 ± 0.78	0.92 ± 0.79	14.1 ± 3.12	15.5 ± 5.08	29.6 ± 5.96
A2	3.39 ± 1.08	1.62 ± 1.26	5.01 ± 1.66	6.69 ± 3.54	5.58 ± 4.01	12.2 ± 5.35

Runs A1 (using a HE MEA) and A2 (using an E-TEK MEA) have the same operating condition.

and five Merck PAH standards) were all less than 5% for all of the analyzed PAHs, while those obtained by replicate analysis were 2–10%. The limits of detection (LODs) of GC/MS were between 0.071 and 0.936 ng for the 21 PAH compounds based on the analyses of serial dilutions of PAH standards. The limit of quantification (LOQ) (= LOD/sampling volume) values of the 21 PAH compounds were 0.076–0.175 ng Nm^{-3}.

RESULTS AND DISCUSSION

Effects of Anode Methanol Flowrate and Concentration on PAHs Emissions

Fig. 2 shows the concentration profiles of gas-phase 21 PAHs collected from the cathode exhaust of fuel cell operated for 6.4 h and then another 6.4 h for stages 1 and 2 (S1 and S2) PAH samplings, respectively, under different anode methanol flow rates (2 and 10 mL min^{-1}), methanol concentration (2 and 4 M), cathode oxygen flow rates (100 and 150 sccm) and temperatures (60°C and 80°C). At methanol concentration = 2 M, methanol flowrate = 2 mL min^{-1}, oxygen flowrate = 150 sccm, and cell temperature = 80°C (standard test condition using HE MEA (run A1)), the emission concentrations of cathode gas-phase PAHs of S1 and S2 ranged from non-detect (ND) (Acp, PA, FL, Pyr, BaA, BbF, BkF, BeP, BghiP, and COR) to 10.3 ± 2.54 (Nap) and ND (NaP, Acp, Flu, PA, FL, Pyr, BaA, CHR, BbF, BkF, BeP, BghiP, and COR) to 0.148 ± 0.047 (IND) μg Nm^{-3}, respectively (Fig. 2(a)). Accordingly, the NaP, Flu, and CHR detected in S1 sampling were not observed in S2 sampling. In addition, the concentration of each detected PAH species was significantly greater in S1 than in S2. Therefore, more PAHs desorption and emission from the cathode in first stage (S1) sampling than in the second stage (S2) sampling. Nap and AcPy were significantly dominant than the other PAH species in S1, while the most predominant PAH species in S2 was IND.

Unlike the trend observed for run A1, PA was the most dominant species among detected PAHs in both S1 (0.195 ± 0.244 μg Nm^{-3}) and S2 (0.894 ± 0.059 μg Nm^{-3}), when the methanol flowrate was raised from 2 to 10 mL min^{-1} (Fig. 2(b)). Furthermore, the concentrations of NaP, AcPy, Acp, Ant, Pyr, BaA, BbF, BkF, BeP, BaP, and BghiP were all below their detection limits in S1, and these PAH species except Ant were also not detected in S2. This phenomenon is possibly attributed to the fact that PAHs usually have smaller Henry's constants or air-water partition coefficients with increasing molecular mass at constant temperature (Shiu and Mackay, 1997), although more desorption of PAHs from carbon materials into the anode methanol and methanol crossover through PEM from anode to cathode at the higher methanol flowrate (fluid convention) might occurred. The methanol crossover is referred to the movement of unreacted methanol from anode to cathode through the membrane in MEA (Kim *et al.*, 2017).

For the same reasons mentioned above, the concentration profile of cathode gas-phase PAHs emission in S1 at the higher methanol concentration of 4 M (run C) (Fig. 2(c)) was quite different from that for run A1 (Fig. 2(a)) or B (Fig. 2(b)). Nevertheless, the PAH concentration profile of S1 was similar to that of S2. The methanol crossover should be enhanced at the greater methanol concentration (Li and Faghri, 2013; Tiwari *et al.*, 2013). Additionally, the water solubility of PAHs approximately decreases with the increase of aromatic ring number, regardless of their low water solubility (ER Wiki, 2017). Through reaction 1, CO_2 could be generated from the methanol oxidation at anode during the operation of DMFC and it might partially emit from the anode due to the air-water exchange of PAH species based on Henry's law (Cheng *et al.*, 2018); nevertheless, it was possible that more CO_2 crossover through the separator might occur at methanol concentration = 4 M, resulting in its release to the surrounding air from the cathode (Jiang and Chu, 2002; Li and Faghri, 2013). The emission concentrations of cathode gas-phase PAHs of S1 and S2 ranged from non-detect (ND) (Ant, Pyr, BaA, BbF, BkF, BeP, BaP, and BghiP) to 3.82 ± 1.20 (Nap) and ND (the same as those of S1 except BaP and BghiP) to 0.353 ± 0.043 (Nap) μg Nm^{-3}, respectively. Hence, the concentrations of individual PAHs of S1 were almost greater than those of S2.

Effects of Cathode Oxygen Flowrate, Cell Temperature, and MEA on PAHs Emissions

At oxygen flowrate of 100 sccm, only CHR, BaP, IND, BbC, and COR were observed in S1, and less PAH species (Ant, CHR, IND, and COR) were detected in S2 (Fig. 2(d)). Of all the detected PAHs, the most dominant species in S1 and S2 were IND (0.208 ± 0.064 μg Nm^{-3}) and Ant (0.035 ± 0.021 μg Nm^{-3}), respectively. When compared to run A1 operated at oxygen flowrate = 150 sccm (Fig. 2(a)), significantly less PAH species and concentration were observed at oxygen flowrate = 100 sccm. Therefore, decreasing the flowrate decreased led to more desorption of PAHs from carbon materials and thus more the PAHs emission from the cathode exhaust, although the strong π-π interaction between PAHs and the graphitic structure of carbon materials should be strong (Kah *et al.*, 2011) and PAHs are relatively easier to adsorb on than to desorb from the surface of carbon blacks (Moninot, 2010).

Fig. 2(e) presents the concentration profiles of 21 individual PAHs in cathode emission gas at 60°C. The concentrations of individual PAHs ranged from ND (Acp, Flu, Pyr, BaA, BbF, BkF, BeP, BaP, and BghiP) to 0.688 ± 0.740 (AcPy) μg Nm^{-3} in S1 and from ND (the same as those of S1 except Acp and Flu) to 1.13 ± 0.60 (NaP) μg Nm^{-3} in S2. For the comparison of operations at 60°C (Fig. 2(e)) and 80°C (Fig. 2(a)), it can be seen that the PAHs emission was lowered with decreasing cell temperature, particularly for low molecular weight ones (e.g., Nap, AcPy, and PA) in both S1 and S2. It is reasonable that the desorption of PAHs should be less at the lower cell temperature. Moreover, the PAHs should be more present in gas-phase than in water-phase because the air-water partition coefficient or Henry's constant of a PAH species increases when temperature rises (Bamford *et al.*, 1999), although methanol crossover increases with increasing temperature (Kumar *et al.*, 2014).

The concentrations of individual PAHs ranged from ND (Pyr, BaA, BbF, BkF, BeP, BaP, PER, IND, DBA, BbC, BghiP,

and COR) to 7.55 ± 6.54 (NaP) and from ND (the same as those of S1 except BaP) to 2.30 ± 0.74 (Acp) μg Nm^{-3} in S1 and S2, respectively (Fig. 2(f)). It is interesting to note that more PAH species were detected for low and middle molecular weight PAHs, but an opposite trend was noticed for high molecular weight PAHs, when the HE MEA installed in the DMFC (run A1) was replaced by an E-TEK one (run A2), although these two runs used the same operating conditions. The difference in cathode Pt loading along with PAH quantity on carbon material might be responsible for the observation.

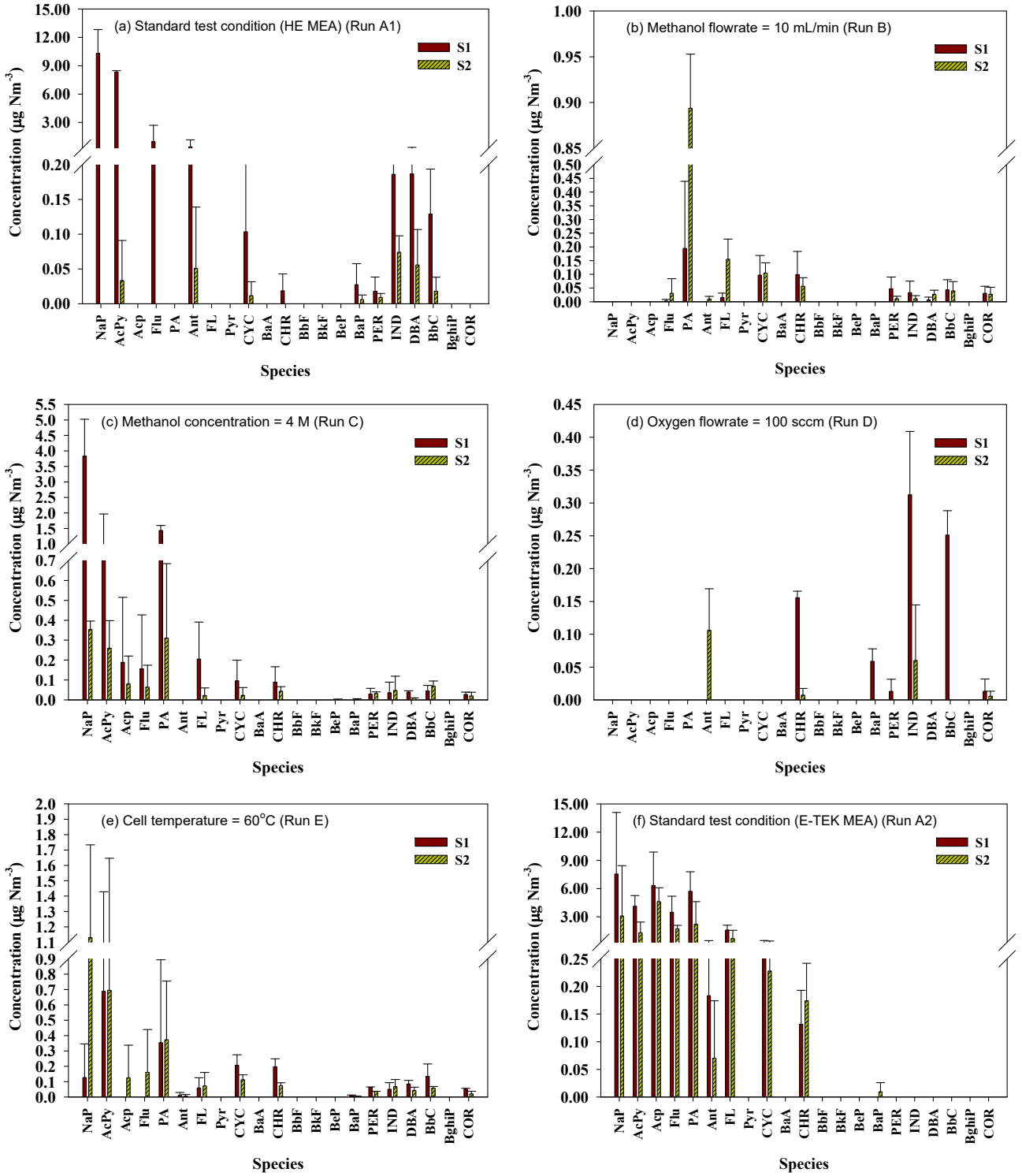

Fig. 2. PAHs concentrations of stage 1 (S1) and S2 of run A1 (methanol flowrate = 2 mL min^{-1}, methanol concentration = 2 M, O_2 flowrate = 150 sccm, and cell temperature = 80°C) (a) and the other runs operated at different operating parameters (b–f) (n = 3).

Comparison of PAH Emission Profiles

For further comparison of the concentration profiles of PAHs obtained in different runs, the concentrations of individual PAHs were normalized to those of corresponding Total-PAHs. The fraction (F) of a PAH species (PAH_i, i = 1–21) can be denoted using the following calculation:

F (%) of PAH_i = 100 × (concentration of PAH_i/concentration of Total-PAHs) (4)

For the standard test condition, the run A1 using a HE MEA had different PAH concentration profiles at S1 (Fig. 3(a)) and S2 (Fig. 3(b)), but the run A2 using an E-TEK MEA showed similar PAH concentration profiles at S1 and S2, which should be resulted from the difference in PAH amount on carbon between the two different MEAs. Various concentration profiles of gas-phase individual PAHs were also seen for the S1 versus S2 of the same run and the S1 versus S1 or S2 versus S2 of different runs with different operating parameters. Nevertheless, the PAH concentration profiles of S1 and S2 were similar for run C which also exhibited more similar PAH concentration profile of S1 to run A1 than the other runs. Therefore, each operating parameter significantly influenced the pattern of PAH concentration profile of S1 or S2. This result might be related to the effect of feeding fuel or gas flowrate or temperature on the PAH water solubility (ER Wiki, 2017) and the gas-water partitioning of individual PAH species (Lee *et al.*, 2004).

Effects of Operating Parameters on Total-PAHs and Total-BaP_{eq} Emissions

At run A1 (standard operation), the concentrations of molecular-weight (MW) classified PAHs for S1 and S2 varied with the order LMW- > HMW- > MMW-PAHs (Fig. 4(a)) and HMW- > LMW- > MMW-PAHs (Fig. 4(b)), respectively. This tendency of S1 (80°C)) at run A1also existed for that at run E (60°C). However, the MW-classified PAHs for runs C and A2 followed the same order (LMW- > MMW- > HMW-PAHs) which was different from those of runs B (HMW- > LMW- > MMW-PAHs) and D (HMW- > MMW- > LMW-PAHs). On the other hand, runs B, C, D, and E exhibited the order LMW- > HMW- > MMW-PAHs in the MW-classified PAHs of S2, different from those of runs A1 (HMW- > LMW- > MMW-PAHs) and A2 (LMW- > MMW- > HMW-PAHs).

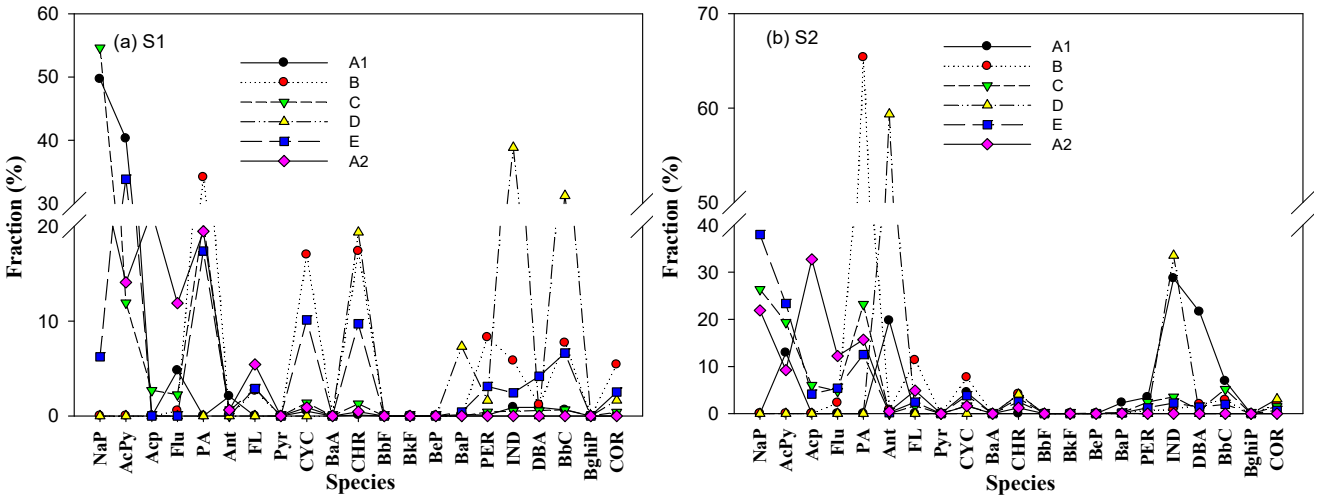

Fig. 3. PAHs concentration fraction profiles (normalized to Total-PAHs concentration) of (a) S1 and (b) S2 at different runs.

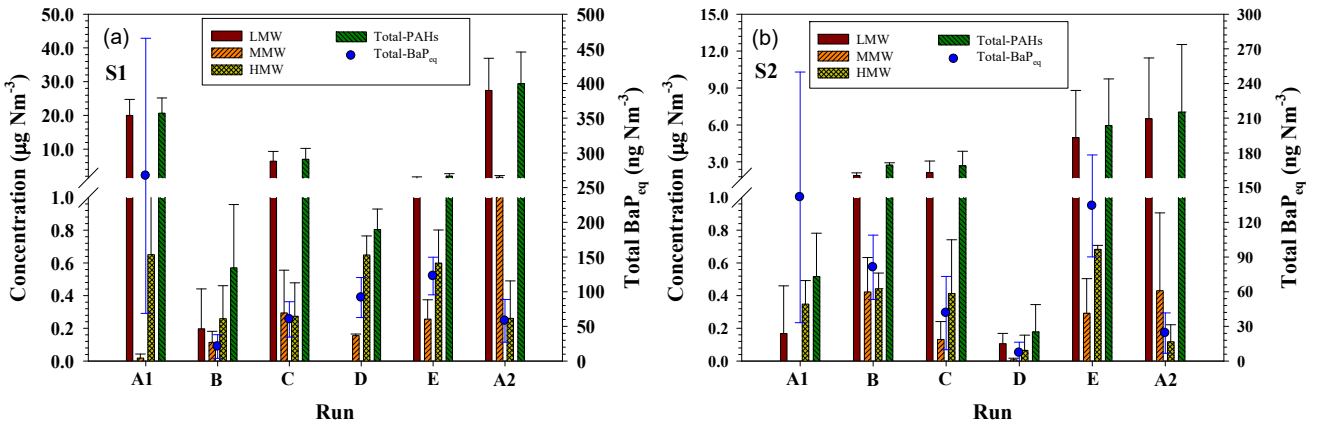

Fig. 4. Concentrations of LMW-, MMW-, HMW-, and Total-PAHs and Total-BaP_{eq} of S1 (a) and S2 (b) at different runs (n = 3).

When using HE MEAs, the Total-PAHs concentrations of these runs were in the order A1 > C > E > D > B for S1, decreasing with the increases of methanol flowrate and concentration or the decreases of oxygen flowrate and cell temperature; however, for S2, this order changed to E > B > C > A1 > D, increasing with the increases of methanol flowrate and concentration or the decrease of cell temperature, but decreasing with the decrease of oxygen flowrate, consistent with our previous work using another E-TEK MEA (Huang *et al.*, 2018). The Total-PAHs concentrations of S1 and S2 were higher for E-TEK MEA (run A2) than for HE MEA (run A1). Consequently, the Total-PAHs concentrations of these runs for S1 + S2 were in the order A2 > A1 > C > E > B > D (36.4 ± 10.9, 21.2 ± 4.48, 9.68 ± 3.44, 7.98 ± 3.85, 3.31 ± 0.43, and 0.98 ± 0.21 μg Nm^{-3}, respectively) (Table 1), decreasing with increasing methanol flowrate and concentration or decreasing oxygen flowrate and cell temperature.

In this study, the benzo(a)pyrene (BaP)-equivalent carcinogenic potency (BaP_{eq}) of a PAH species was calculated from the product of its toxic equivalence factor (TEF) and concentration (Nisbet and LaGoy, 1992). The PAH-derived Total-BaP_{eq} concentrations, followed the orders A1 > E > D > C > B for S1 (Fig. 4(a)) and A1 > E > B > C > D (Fig. 4(b)) for S2. As a result, the Total-BaP_{eq} concentrations of these runs of S1 + S2 were in the order A1 > E > B ≈ C > D (409 ± 226, 257 ± 51.7, 102 ± 32.6, 102 ± 40.7, and 98.7 ± 30.3 ng Nm^{-3}, respectively) (Table 1), also decreasing with increasing methanol flowrate and concentration or decreasing oxygen flowrate and cell temperature. The Total-BaP_{eq} concentrations of S1 and S2 were both greater for run A1 than for run A2, so The Total-BaP_{eq} concentration of S1 + S2 was higher for run A1 than for run A2 (82.3 ± 35.3 ng Nm^{-3}) (Table 1). This result is majorly attributed to the difference in concentration for PAH species (BaP and DBA) with TEF = 1.

Polarization Curves and Emission Factors

For the DMFC installed with similar HE MEAs in different runs, the polarization (current-potential) curves in Fig. 5(a) shows that runs A1, B, C, and D had similar cell performances, but the cell performance decreased as cell temperature decreased from 80°C to 60°C. This finding is coincident with the fact that the performance of a DMFC increases with an increase in cell temperature, although methanol crossover also increases with increasing temperature (Bahrami and Faghri, 2013; Kumar *et al.*, 2014). Furthermore, the impedance responses (containing both real (Z') and imaginary (–Z") components) in Fig. 5(b) presents that the activation impedances of runs A1, B, C, and D were similar but significantly lower than that of run E, also supporting the result of polarization test in Fig. 5(a).

Table 1 summarizes the emission factors (EFs) of gas-phase Total-PAHs and Total-BaP_{eq} for S1 and S2 and their sums (S1 + S2) under different operating variables. The Total-PAHs EFs of different runs varied from 0.06 ± 0.02 to 2.38 ± 0.52 and from 0.01 ± 0.02 to 0.69 ± 0.78 μg g-electrode^{-1} for S1 and S2, respectively, while those of S1+S2 ranged from 0.07 ± 0.03 to 2.44 ± 0.52 μg g-electrode^{-1}, decreasing with increasing methanol flowrate and concentration or decreasing oxygen flowrate and cell temperature. A similar trend was also observed for the EFs of Total-BaP_{eq} with the ranges of (2.42 ± 1.96)−(30.8 ± 22.8), (0.55 ± 0.71)−(16.3 ± 12.5), and (7.58 ± 2.32)−(47.1 ± 26.0) ng g-electrode^{-1}, for S1, S2, and S1+S2, respectively. When operating at the same condition, the EFs of Total-PAHs of S1, S2, and S1 + S2 for run A1 using HE MEA were all smaller than those of run A2 using E-TEK MEA, opposite to the tendency for their EFs of Total-BaP_{eq}. This phenomenon should be related to the greater cathode Pt-loading needing more carbon support and GDL materials and the difference in concentration for high TEF PAH species (BaP and DBA).

For comparison purpose, a power-based emission factor can be used when considering those used for general power generators; however, it is likely that the emission concentration of gas-phase Total-PAHs of DMFC may diminish to ND after operation for a period of time. To reduce the gas-phase Total-PAHs emission of DMFC, the operating condition of run D is suggested because it had the lowest EFs of Total-PAHs and Total-BaP_{eq} among the tested runs, although its cell performance was slightly lower than that of run A1 (standard test condition).

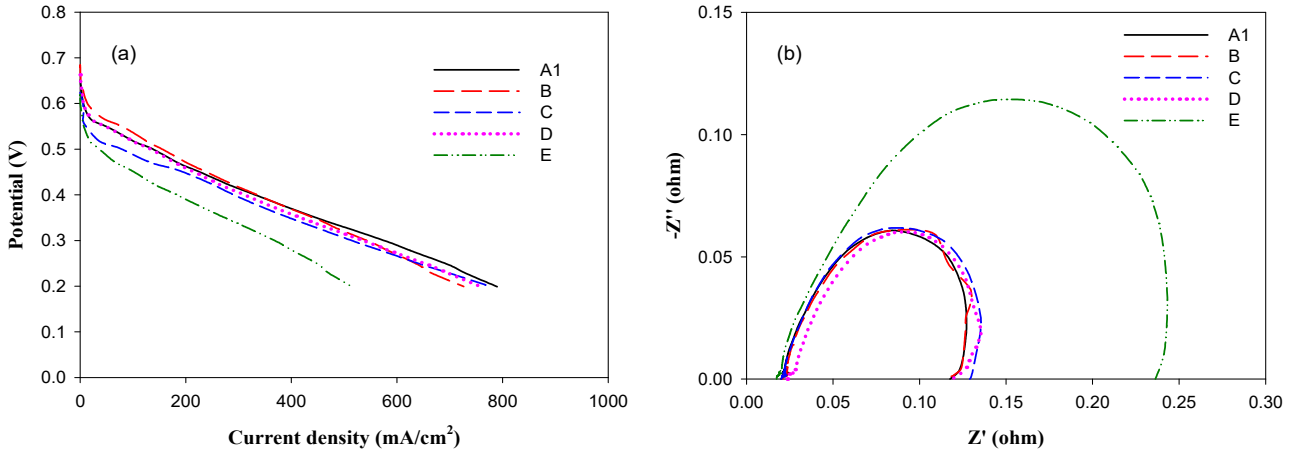

Fig. 5. (a) Cell potential versus current density (I–V) curves and (b) AC impedance Nyquist plotsat 0.5 V (10 K–0.01 Hz) curves for the HE MEAs installed in DMFC operated at different runs (A1–E).

CONCLUSIONS

In this study, at the standard test condition (run A1), the emission concentrations of cathode gas-phase PAHs of S1 and S2 ranged from ND to 10.3 ± 2.54 (Nap) and ND to 0.148 ± 0.047 (IND) μg Nm^{-3}, respectively. More PAH species were detected the cathode in S1 than in S2. The Total-PAHs and Total-BaP_{eq} concentrations of S1 + S2 were 21.2 ± 4.48 μg Nm^{-3} and 409 ± 226 ng Nm^{-3}, respectively.

The run A1 using a HE MEA had different PAH concentration profiles of S1 and S2, but the run A2 using an E-TEK MEA showed similar PAH concentration profiles of S1 and S2. Each operating parameter significantly influenced the pattern of PAH concentration profile of S1 or S2. The concentrations of molecular-weight (MW) classified PAHs for S1 and S2 varied with the order LMW- > HMW- > MMW-PAHs and HMW- > LMW- > MMW-PAHs, respectively. The Total-PAHs and Total-BaP_{eq} concentrations of different runs for S1+S2 were in the order A2 > A1 > C > E > B > D (36.4±10.9)–(0.98±0.21) μg Nm^{-3} and A1 > E > B ≈ C > D (409 ± 226)–(98.7 ± 30.3) ng Nm^{-3}, respectively, decreasing with increasing methanol flowrate and concentration or decreasing oxygen flowrate and cell temperature.

Runs A1, B, C, and D had similar cell performances, but the cell performance decreased as cell temperature decreased from 80°C to 60°C. The EFs of Total-PAHs and Total-BaP_{eq} of S1+S2 for different runs ranged from 0.07 ± 0.03 to 2.44 ± 0.52 μg g-$electrode^{-1}$ and from 7.58 ± 2.32 to 47.1 ± 26.0 ng g-$electrode^{-1}$, also decreasing with increasing methanol flowrate and concentration or decreasing oxygen flowrate and cell temperature. At the same operating condition, run A1 emitted more Total-PAHs and Total-BaP_{eq} than run A2.

ACKNOWLEDGEMENT

The authors would like to thank the Ministry of Science and Technology, Taiwan, R.O.C. for financially supporting this research under Grant Nos. MOST 96-2211-E-020-011-MY2 and 106-2221-E-020-003-MY3.

REFERENCES

Bahrami, H. and Faghri, A. (2013). Review and advances of direct methanol fuel cells: Part II: Modeling and numerical simulation. *J. Power Sources* 230: 303–320.

Cheng, J.O., Ko, F.C., Lee, C.L. and Fang, M.D. (2013). Air–water exchange fluxes of polycyclic aromatic hydrocarbons in the tropical coast, Taiwan. *Chemosphere* 90: 2614–2622.

Dat, N.D., Lyu, J.M. and Chang, M.B. (2018). Variation of atmospheric PAHs in northern Taiwan during winter and summer seasons. *Aerosol Air Qual. Res.* 18: 1019–1031.

Deng, G., Liang, L., Li, C., Ge, J., Liu, C., Jin, Z. and Xing, W. (2019). Mass transport in anode gas diffusion layer of direct methanol fuel cell derived from compression effect. *J. Power Sources* 427: 120–128.

ER Wiki (2017). Polycyclic Aromatic Hydrocarbons (PAHs), http://www.environmentalrestoration.wiki/index.php?title=Polycyclic_Aromatic_Hydrocarbons_(PAHs). Last Access: 10 July 2017.

Falcão, D.S., Oliveira, V.B., Rangel, C.M. and Pinto, A.M.F.R. (2014). Review on micro-direct methanol fuel cells. *Renewable Sustainable Energy Rev.* 34: 58–70.

Fan, Z.L., Chen, X.C., Lui, K.H., Ho, S.S.H., Cao, J.J., Lee, S.C., Huang, H. and Ho, K.F. (2017). Relationships between outdoor and personal exposure of carbonaceous species and polycyclic aromatic hydrocarbons (PAHs) in fine particulate matter ($PM_{2.5}$) at Hong Kong. *Aerosol Air Qual. Res.* 17: 666–679.

Huang, K.L., Lai, Y.C. and Tsai, C.H. (2006). Effects of sputtering parameters on the performance of electrodes fabricated for proton exchange membrane fuel cells. *J. Power Sources* 156: 224–231.

Huang, K.L., Tsai, T.H., Tsai, J.H., Chen, S.J., and Lee, W.J. (2015). Emission of PAHs from a single hydrogen-oxygen PEM fuel cell: In relation to fuel cell carbon materials. *Aerosol Air Qual. Res.* 15: 2654–2667.

Huang, K.L., Wu, M.S., Tsai, J.H., Lin, D.Y., Chen, S.J. and Lee, W.J. (2016). Effect of operating conditions on PAHs emission from a single H_2-O_2 PEM fuel cell. *Aerosol Air Qual. Res.* 16: 2186–2197.

Huang, K.L., Tsai, T.H., Chen, S.J., Chao, H.R., Kuo, Y.M. and Tsai, J.H. (2018). Gas- and water-phase PAHs emitted from a single hydrogen-oxygen PEM fuel Cell. *Aerosol Air Qual. Res.* 18: 2654–2667.

Jiang, P., Yang, L., Chen, X., Gao, Y., Li, Y., Zhang, J., Zhao, T., Yu, H. and Wang, W. (2018). Impact of dust storms on NPAHs and OPAHs in $PM_{2.5}$ in Jinan, China, in spring 2016: Concentrations, health risks, and sources. *Aerosol Air Qual. Res.* 18: 471–484.

Joghee, P., Malik, J.N., Pylypenko, S. and O'Hayre, R. (2015). A review on direct methanol fuel cells – In the perspective of energy and sustainability. *MRS Energy & Sustainability* 2: 1–31.

Kah, M., Zhang, X., Jonker, M.T. and Hofmann, T. (2011) Measuring and modeling adsorption of PAHs to carbon nanotubes over a six order of magnitude wide concentration range. *Environ. Sci. Technol.* 45: 6011–6017.

Kim, S., Jang, S., Kim, S.M., Ahn, C.Y., Hwang, W., Cho, Y.H., Sung, Y.E. and Choi, M. (2017). Reduction of methanol crossover by thin cracked metal barriers at the interface between membrane and electrode in direct methanol fuel cells. *J. Power Sources* 363:153–160.

Kumar, P., Dutta, K., Das, S. and Kundu, P.P. (2014). An overview of unsolved deficiencies of direct methanol fuel cell technology: Factors and parameters affecting its widespread use. *Int. J. Energy Res.* 38: 1367–1390.

Lai, Y.C., Huang, K.L., Tsai, C.H., Lee, W.J. and Chen, Y.L. (2012). Sputtered Pt loadings of membrane electrode assemblies in proton exchange membrane fuel cells. *Int. J. Energy Res.* 32: 918–927.

Lai, Y.C., Tsai, C.H., Chen, Y.L. and Chang-Chien, G.P. (2017). Distribution and sources of atmospheric polycyclic aromatic hydrocarbons at an industrial region in Kaohsiung, Taiwan. *Aerosol Air Qual. Res.* 17: 776–787.

Lee, D. and Lee, D.G. (2016). Carbon composite bipolar plate for high-temperature proton exchange membrane fuel cells (HT-PEMFCs). *J. Power Sources* 327: 119–126.

Lee, J.J., Huang, K.L., Yu, Y.Y. and Yang, S.C. (2004). Laboratory retention of vapor-phase PAHs using XAD adsorbents. *Atmos. Environ.* 38: 6185–6193.

Li, X. and Faghri, A. (2013). Review and advances of direct methanol fuel cells (DMFCs) Part I: Design, fabrication, and testing with high concentration methanol solutions. *J. Power Sources* 226: 223–240.

Li, Y.Y., Yang, L.X., Chen, X.F., Gao, Y., Jiang, P., Zhang, J.M., Yu, H. and Wang, W.X. (2017). $PM_{2.5}$-bound PAHs in indoor and outdoor of hotels in urban and suburban of Jinan, China: Concentrations, sources, and health risk impacts. *Aerosol Air Qual. Res.* 17: 2463–2473.

Mansor, M., Timmiati, S.N., Lim, K.L., Wong, W.Y., Kamarudin, S.K. and Kamarudin, N.H.N. (2019). Recent progress of anode catalysts and their support materials for methanol electrooxidation reaction. *Int. J. Hydrogen Energy* 44: 14744–14769.

Mario, A., Mihaela, M., Massimo, D. and Maurizio, G. (2018). Impact of emissions, meteorology and grid resolution on changes in HMs and PAHs concentrations between 2005 and 2010 in Italy. *Aerosol Air Qual. Res.* 18: 3165–3176.

Nakagawa, N., Sekimoto, K., Masdar, M.S. and Noda, R. (2009). Reaction analysis of a direct methanol fuel cell employing a porous carbon plate operated at high methanol concentrations. *J. Power Sources* 186: 45–51.

Nisbet, C. and LaGoy, P. (1992). Toxic equivalency factors (TEFs) for polycyclic aromatic hydrocarbons (PAHs). *Regul. Toxicol. Pharm.* 16: 290–300.

Saha, M., Maharana, D., Kurumisawa, R., Takada, H., Yeo, B.G., Rodrigues, A.C., Bhattacharya, B., Kumata, H., Okuda, T., He, K., Ma, Y., Nakajima, F., Zakaria, M.P., Giang, D.H. and Viet, P.H. (2017). Seasonal trends of atmospheric PAHs in five Asian megacities and source detection using suitable biomarkers. *Aerosol Air Qual. Res.* 17: 2247–2262.

Siudek, P. and Frankowski, M. (2018). The role of sources and atmospheric conditions in the seasonal variability of particulate phase PAHs at the urban site in central Poland. *Aerosol Air Qual. Res.* 18: 1405–1418.

Tenson, T.J. and Baby, R. (2017). Recent advances in proton exchange membrane fuel cells: A review. *IJARSET* 4: 34–40.

Tiwari, J.N., Tiwari, R.N., Singh, G. and Kim, K.S. (2013). Recent progress in the development of anode and cathode catalysts for direct methanol fuel cells. *Nano Energy* 2: 533–578.

Tran, P.D., Morozan, A., Archambault, S., Heidkamp, J., Chenevier, P., Dau, H., Fontecave, M., Martinent, A., Jousselme, B. and Artero, V. (2015). A noble metal-free proton-exchange membrane fuel cell based on bio-inspired molecular catalysts. *Chem. Sci.* 6: 2050–2053.

Tsukagoshi, Y., Ishitobi, H. and Nakagawa, N. (2018). Improved performance of direct methanol fuel cells with the porous catalyst layer using highly-active nanofiber catalyst. *Carbon Resour. Convers.* 1: 61–72.

Wang, J., Guinot, B., Dong, Z., Li, X., Xu, H., Xiao, S., Ho, S.S.H., Liu, S. and Cao, J. (2017). $PM_{2.5}$-bound polycyclic aromatic hydrocarbons (PAHs), oxygenated-PAHs and phthalate esters (PAEs) inside and outside middle school classrooms in Xi'an, China: Concentration, characteristics and health risk assessment. *Aerosol Air Qual. Res.* 17: 1811–1824.

Wasmus, S. and Küver, A. (1999). Methanol oxidation and direct methanol fuel cells: A selective review. *J. Electroanal. Chem.* 461: 14–31.

Wright, L.P., Zhang, L., Cheng, I., Aherne, J. and Wentworth, G.R. (2018). Impacts and effects indicators of atmospheric deposition of major pollutants to various ecosystems - A review. *Aerosol Air Qual. Res.* 18: 1953–1992.

Xu, S., Chen, T., Li, X., Yan, J. and Cen, K. (2018). Behavior of PCDD/Fs, PCBs, CBzs and PAHs during thermal treatment of various fly ash from steel industry. *Aerosol Air Qual. Res.* 18: 1008–1018.

Zeis, R. (2015). Materials and characterization techniques for high-temperature polymer electrolyte membrane fuel cells. *Beilstein J. Nanotechnol.* 6: 68–83.

Zhang, N., Cao, J., Li, L., Ho, S.S.H., Wang, Q., Zhu, C. and Wang, L. (2018). Characteristics and source identification of polycyclic aromatic hydrocarbons and *n*-alkanes in $PM_{2.5}$ in Xiamen. *Aerosol Air Qual. Res.* 18: 1673–1683.

Received for review, August 12, 2019
Revised, August 26, 2019
Accepted, September 6, 2019